Bioprocess Biosyst Eng
DOI 10.1007/s00449-013-0931-5

ORIGINAL PAPER

Construction of an improved amperometric acrylamide biosensor based on hemoglobin immobilized onto carboxylated multi-walled carbon nanotubes/iron oxide nanoparticles/chitosan composite film

Bhawna Batra · Suman Lata · C. S. Pundir

Received: 10 November 2012 / Accepted: 12 February 2013

Abstract A method is described for construction of an improved amperometric acrylamide biosensor based on covalent immobilization of hemoglobin (Hb) onto nanocomposite of carboxylated multi-walled carbon nanotubes (cMWCNT) and iron oxide nanoparticles (Fe_3O_4NPs) electrodeposited onto Au electrode through chitosan (CHIT) film. The Hb/cMWCNT-Fe_3O_4NP/CHIT/Au electrode was characterized by scanning electron microscopy, Fourier transform infra-red spectroscopy, electrochemical impedance spectroscopy, and differential pulse voltammetry at different stages of its construction. The biosensor was based on interaction between acrylamide and Hb, which led to decrease in the electroactivity of Hb, i.e., current generated during its reversible conversion [Fe(II)/Fe(III)]. The biosensor showed optimum response within 8 s at pH 5.0 and 30 °C. The linear working range for acrylamide was 3–90 nM, with a detection limit of 0.02 nM and sensitivity of 36.9 μA/nM/cm^2. The biosensor was evaluated and employed for determination of acrylamide in potato crisps.

Keywords Acrylamide · Biosensor · Hemoglobin · Chitosan · Carboxylated multi-walled carbon nanotubes · Potato crisps

Introduction

Acrylamide, a neurotoxin and potential carcinogen, is formed during high-temperature (>120 °C) cooking of many commonly consumed foods [1, 2]. It is derived from the reaction between reducing sugars and proteins/amino-acids (mainly asparagine) [3]. Different factors such as oil type and amount [5], the glucose–asparagine ratio [6], storage practices during potato frying [7] influence acrylamide formation and its content in food. A very high amount of this toxic compound has been found in potato chips, levelling up to 4 mg/kg [4]. Acrylamide has also been found to react with DNA to act as human carcinogen [1]. Various analytic methods available for quantification of acrylamide in food products such as liquid chromatography–tandem mass spectrometry (LC–MS/MS) [8], gas chromatography–mass spectrometry (GC–MS) [9], high-performance liquid chromatography–mass spectrometry (HPLC–MS) [10], and ultra high-performance liquid chromatography-tandem mass spectrometry (UHPLC-MS/MS) [11], are expensive and time-consuming. Hence, there is a growing demand for alternative method for rapid and precise screening of acrylamide. The biosensors offer great promise for detection of biomolecules with simplicity, rapidity, and high sensitivity. Two voltammetric acrylamide biosensors employing hemoglobin-dimethyldioctadecylammonium bromide (Hb-DDAB) modified carbon paste electrode [12], glassy carbon (GC) electrodes modified with single-walled carbon nanotubes (SWCNT)/hemoglobin (Hb) [13], and an amperometric acrylamide biosensor based on immobilization of Hb onto cMWCNT/CuNPs/PANI hybrid film [14] have been reported. All these biosensors rely on the reaction of hemoglobin with acrylamide, which leads to the creation of a hemoglobin–acrylamide adduct, this adduct alters the electroactivity of Hb. Four iron heme prosthetic groups of Hb are responsible for its electroactivity undergoing the reversible conversion of Fe(II)/Fe(III). Hb is susceptible to both reversible and irreversible modification: the sixth position of iron can be occupied by a

B. Batra · S. Lata · C. S. Pundir (✉)
Department of Biochemistry, M.D. University, Rohtak 124001, India
e-mail: chandraspundir@gmail.com

Published online: 14 March 2013

ligand. As the adduct hemoglobin–acrylamide concentration increases at the electrode surface, the current peak of differential pulse voltammogram (DPV) would decrease. Thus, the decrease in current was treated as the analytical signal for acrylamide content in these biosensors.

Chitosan (CHIT) is a very attractive polysaccharide due to its reported low toxicity, biodegradability, and mucoadhesivity [15]. It is a cationic polysaccharide obtained by partial deacetylation of chitin, the major component of crustacean shells. In contrast to other polymers, CHIT is a hydrophilic polymer with positive charge that comes from weak basic groups, which give it special characteristics from the technological point of view. CHIT has been extensively used for the immobilization of enzymes and thus construction of biosensors due to its excellent characteristics such as biocompatibility, film forming ability, physiological inertness, and high mechanical strength [16].

Iron oxide nanoparticles (Fe_3O_4NP) are a kind of nanomaterial, which have a very large surface area and good biocompatibility and hence employed for construction of various electrochemical biosensors [17]. Carbon nanotubes (CNT) have established themselves as a good material for immobilization of enzymes/proteins due to their unique physical properties, including high electrical conductivity, superior chemical and mechanical stability, and large surface area as cMWCNT could keep enzyme/protein activity due to the desirable microenvironment and enhance the direct electron transfer between the enzyme's active sites and the electrode. The present report describes the construction of an improved amperometric acrylamide biosensor by immobilizing hemoglobin onto nanocomposite of cMWCNT and Fe_3O_4NPs electrodeposited onto Au electrode through chitosan film.

Materials and methods

Materials

Hemoglobin human (Hb) from Sigma-Aldrich St. Louis, USA, carboxylated multi-walled carbon nanotubes (cMWCNT) (Functionalized MWCNT) from Intelligent Materials Pvt. Ltd. Panchkula (Haryana) India, sodium chloride (NaCl), hexane, acrylamide, chitosan, potassium hexacyanoferrate (II) trihydrate (Carrez I), acetic acid, zinc sulphate heptahydrate (Carrez II), *N*-ethyl-*N*'-(3-dimethylaminopropyl) carbodiimide (EDC), *N*-hydroxy succinimide (NHS) from SISCO Research Lab., Mumbai, India were used. Double distilled water (DW) was used throughout the experimental studies.

Apparatus used

Potentiostat/Galvanostat (Make: Autolab, model: AUT 83785, manufactured by Eco Chemie) with a three electrode system composed of a Pt wire as an auxillary electrode, an Ag/AgCl electrode as reference electrode and Hb/cMWCNT-Fe_3O_4NP/CHIT modified Au electrode as a working electrode, transmission electron microscope (TEM) (JEOL 2100 F) and scanning electron microscope (SEM) (Zeiss EV040), UV spectrophotometer (Make: Shimadzu, Model 160 A), X-ray diffractometer (XRD) (Make: 122 Rigaku, D/Max2550, Tokyo, Japan), Fourier transform Infra-red spectrophotometer (FTIR) (Thermo Scientific, USA).

Construction of Hb/cMWCNT/Fe_3O_4NP/CHIT modified Au electrode

Preparation of Fe_3O_4NP

Fe_3O_4NP were prepared by co-precipitation of Fe(II) and Fe(III) as described in [18] with slight modification. Five milliliters of iron ion solution containing 0.25 M Fe^{2+} and Fe^{3+} (1:1 ratio) were added dropwise into 50 ml NaOH (2 M) solution under vigorous mechanical stirring for 35 min at 80 °C. The precipitates were washed first with DW and then ethanol 2–3 times and collected by applying external magnetic field until the supernatant solution turned neutral. The resulting Fe_3O_4NPs were dried in oven at 70 °C. The morphology, particle size, and structure of the Fe_3O_4NP were determined by TEM.

Electrodeposition of cMWCNT-Fe_3O_4NP/CHIT onto Au electrode

The surface of a Au electrode (2 cm × 1 mm) was polished manually by alumina slurry (diameter 0.05 μm) with a polishing cloth, followed by thorough washing with DW and then placed into ethanol, sonicated to remove adsorbed particles, and finally washed 3–4 times with DW. The cMWCNT(1.0 mg) were suspended into 4 ml mixture of concentrated H_2SO_4 and HNO_3 in 3:1 ratio and ultrasonicated for 3–4 h to get its finely dispersed black colored solution. The dispersed cMWCNT solution (0.1 ml) was mixed into a mixture of 0.5 ml EDC (0.2 M) and 0.5 ml NHS (0.2 M). The pH was adjusted to 6.0 and kept at RT for 1 h. Chitosan (200 μl) was added to 25.0 ml of 1 N KCl and electropolymerized onto Au electrode through cyclic voltammetry by applying 20 successive polymerization cycles at −0.1 to 0.2 V. Fe_3O_4NP suspension (200 μl) and 1.0 ml of cMWCNT suspension were added into 25 ml 1 N KCl and finally electrodeposited onto the Au electrode by applying 20 polymerization cycles at −0.1 to 0.2 V. During the electrochemical polymerization, the surface of Au electrode became green gradually, indicating the deposition of cMWCNT-Fe_3O_4NP/CHIT film on Au wire. The resulting cMWCNT-Fe_3O_4NP/CHIT-modified

gold electrode was washed thoroughly with DW to remove unbound matter and kept in a dry Petri-plate at 4 °C.

Immobilization of Hb onto cMWCNT/Fe_3O_4NP/CHIT-modified Au electrode

cMWCNT-Fe_3O_4NP/CHIT/Au electrode was placed into 2 ml of haemoglobin solution (0.1 mM) and kept overnight at room temperature for immobilization. The resulting bioelectrode (Hb/cMWCNT-Fe_3O_4NP/CHIT/Au electrode) was washed 3–4 times with 0.2 M sodium acetate buffer, pH 5.0 to remove unbound protein and used as a working electrode. It was stored at 4 °C when not in use. The working electrode was characterized by SEM, FTIR, and EIS at different stages of its construction.

Differential pulse voltammetry measurement and testing of acrylamide biosensor

Differential pulse voltammetry of Hb/cMWCNT-Fe_3O_4NP/CHIT Au electrode was recorded in Potentiostat–Galvanostat from 0.075 to 0.275 V versus Ag/AgCl as reference and Pt wire as counter electrode in a 30 ml of 0.2 M sodium acetate buffer (pH 5.0) containing 100 µl of 3.5 µM acrylamide.

Optimization of acrylamide biosensor

To optimize the working conditions of the present biosensor, effects of pH, incubation temperature, time and substrate (acrylamide) concentration on biosensor response were recorded. To determine optimum pH, the pH was varied between pH 4.0 and 8.0 at an interval of pH 0.5 using the following buffer, each at a final conc. of 0.2 M: pH 4.0–6.0 sodium acetate buffers and pH 6.5–8.0 sodium phosphate buffers. Similarly to determine optimum temperature, the reaction mixture was incubated at different temperature (20–50 °C at an interval of 5 °C). The effect of acrylamide concentration on biosensor response was determined in the concentration range 3–130 nM. LOD was calculated as the lowest quantity of substrate (acrylamide) required to give a signal equal to background + (blank) 3 times of SD of blank. Sensitivity was calculated as change in current after addition of one unit concentration of substrate (acrylamide) per unit area of electrode.

Amperometric determination of acrylamide in potato crisp

Crushed potato crisps of different make (4 g) were ground to powder in pestle mortar. The powder was mixed into DW (100 ml) and kept for swelling at room temperature. After 20 min, the sample was stirred at 60 °C for 1 h and then centrifuged at 4,500 rpm for 20 min. The supernatant was collected and defatted by extraction in hexane. The obtained aqueous solution was purified by adding Carrez I and Carrez II (2.5 ml). The supernatant was subsequently filtered and its acrylamide content was measured by the present biosensor in the similar manner as described for its response measurement under the optimal working conditions except the acrylamide was replaced by potato crisp water extract. The acrylamide content in the potato crisp was interpolated from standard curve between acrylamide concentration (nM) versus current (µM) (Fig. 1).

Storage stability of Hb/cMWCNT-Fe_3O_4NP/CHIT/Au electrode

The stability of the working electrode was studied for 2 months by measuring its response weekly. The present electrode system was stored in dried condition at 4 °C when not in use.

Results and discussion

Characterization of Fe_3O_4NP

The characterization of nanoparticles was carried out by UV and visible, TEM, XRD, and FTIR spectroscopy (Fig. 2a–d). UV and visible spectra exhibited strong absorbance peak at 300 nm, confirming the synthesis of Fe_3O_4NP (Fig. 2a). The typical TEM images of Fe_3O_4NP nanoparticles (Fig. 2b) showed the spherical shape of Fe_3O_4NP with an average size of 20 nm. The XRD patterns of the prepared NPs clearly showed the characteristics peaks of Fe_3O_4NP at 24.8°, 33.4°, 36.7°, 42.3°, 50.2°, 54.3°, 58.1°, 64.2°, and 65.4° (Fig. 2c). No characteristic peaks of impurities were observed, revealing the high purity of the Fe_3O_4NP. All peaks were consistent with the peaks of Fe_3O_4NP with high crystallinity. The FTIR spectrum of the Fe_3O_4NP nanoparticles exhibited absorption peaks at 3,448.33 and 1,632.00 cm^{-1} (Fig. 2d) assigned to the Fe_3O_4NP stretching vibration mode, which confirms the formation of Fe_3O_4NP.

SEM studies of Au electrode during modification

The SEM images of the surface of bare Au electrode, cMWCNT-Fe_3O_4NP/CHIT/Au electrode and Hb/cMWCNT-Fe_3O_4NP/CHIT/Au electrode are shown in Fig. 3a–c, respectively. The stepwise modification of electrode could be seen clearly from these SEM images. The SEM image of the bare Au electrode showed a smooth and featureless morphology. The cMWCNT-Fe_3O_4NP/

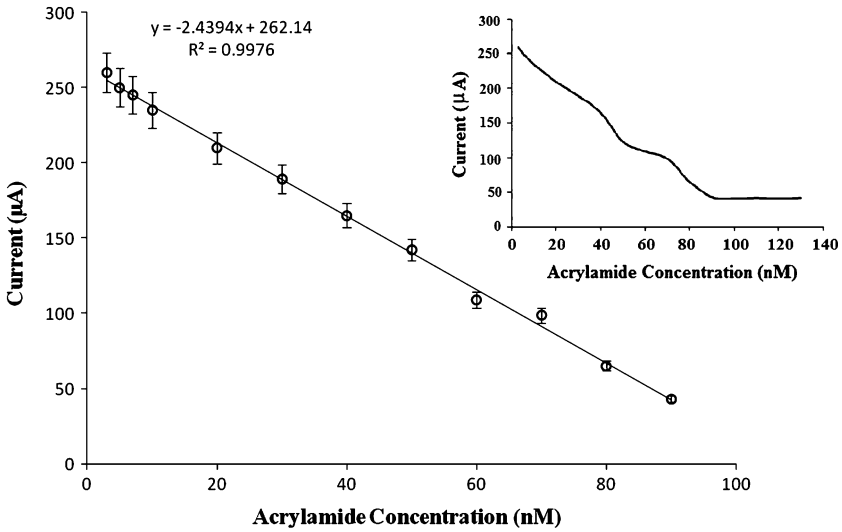

Fig. 1 Effect of acrylamide concentration on response of acrylamide biosensor based on Hb/cMWCNT-Fe_3O_4NP/CHIT/Au electrode

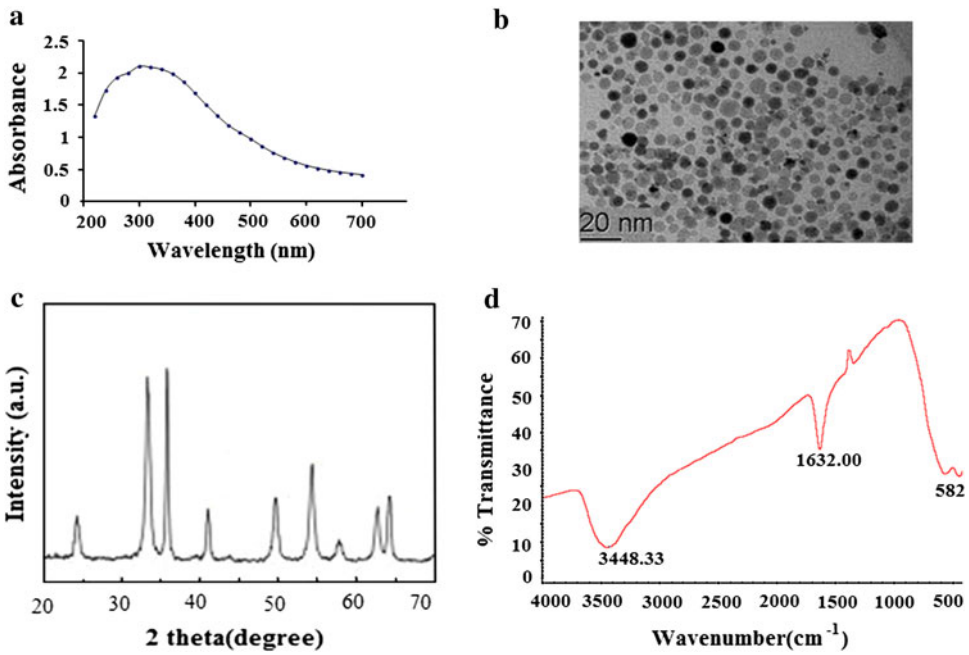

Fig. 2 **a** Ultra-violet and visible spectrum of Fe_3O_4NP, **b** transmission electron microscopic images, of Fe_3O_4NP and **c** X-ray diffraction pattern of taken from Fe_3O_4NP, **d** Fourier transform infra red spectrum of Fe_3O_4NP

CHIT/Au composite film exhibited a net structure, i.e., film which is more uniform and porous, hence provides larger effective surface area. The globular structural morphology of Hb/cMWCNT-Fe_3O_4NP/CHIT/Au changes into the regular form due to immobilization of Hb onto cMWCNT-Fe_3O_4NP/CHIT/Au electrode.

Construction of acrylamide biosensor

Figure 4 summarizes the construction of acrylamide biosensor based on immobilization of Hb on nanocomposite film of Fe_3O_4NP and cMWCNT electrodeposited onto CHIT film decorated Au electrode. First, CHIT was electropolymerized on the surface of Au electrode, as this method is easy and the layer thickness could be controlled and then cMWCNT and Fe_3O_4NP were co-electrodeposited on the CHIT coated Au electrode. To construct the working electrode, Hb was immobilized covalently onto cMWCNT-Fe_3O_4NP/CHIT/Au electrode. Incubation of Hb solution with activated cMWCNT-Fe_3O_4NP/CHIT/Au electrode leads to effective collision between –COOH group of cMWCNT and $–NH_2$ groups on the surface of the Hb to form an amide (–CO–NH) bond through EDC and NHS chemistry. EDC and NHS activate the free –COOH groups of cMWCNT-Fe_3O_4NP/CHIT composite layer. The CV study was carried for Hb/cMWCNT-Fe_3O_4NP/CHIT/Au electrode at different scan rates in the range 10–50 mV/s at interval of 10 mV/s, the optimum current was obtained

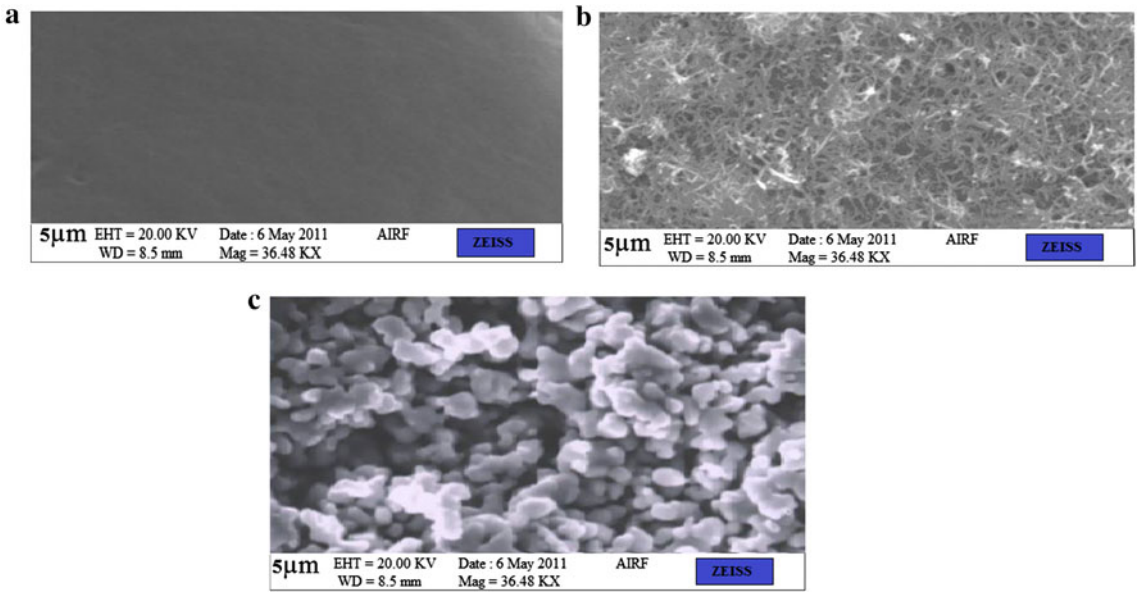

Fig. 3 Scanning electron microscopic images of **a** bare Au electrode **b** cMWCNT-Fe_3O_4NP/CHIT/Au electrode Au electrode and **c** Hb/cMWCNT-Fe_3O_4NP/CHIT/Au electrode

at 20 mV/s and hence for subsequent CV studies were performed at 20 mV/s (Fig. 5). The CV of cMWCNT-Fe_3O_4NP/CHIT/Au exhibited higher currents than CHIT/Au, which indicate that cMWCNT-Fe_3O_4NP/CHIT/Au composite film, have large effective surface area than CHIT/Au. cMWCNT-Fe_3O_4NP/CHIT/Au composite film could provide a conducting path through the composite matrix for faster kinetics (Fig. 6). Hence, the cMWCNT-Fe_3O_4NP, acting as electron transfer mediator help in enhancing the biosensor response and thus increase its sensitivity.

FTIR spectra

Figure 7A shows FTIR spectra for CHIT/Au electrode (curve i), cMWCNT-Fe_3O_4NP/CHIT/Au electrode (curve ii) and Hb/cMWCNT-Fe_3O_4NP/CHIT/Au electrode (curve iii). FTIR spectra of electrodeposited CHIT/Au composite showed bands at 1,000–1,750 cm^{-1} (curve i) due to the stretching vibration mode of –OH and $–NH_2$ group. The peak at 1,745 cm^{-1} is assigned to C–O stretching, 1,650 cm^{-1} is attributed to amide I group (C–O stretching along with N–H deformation mode), and 1,096 cm^{-1} to the stretching vibration mode of the hydroxyl group. Curve (ii) shows the FTIR spectra of cMWCNT-Fe_3O_4NP/CHIT/Au electrode, which showed several significant peaks. The peak at 582 cm^{-1} belonging to the stretching vibration mode of Fe–O bond. The FTIR spectra of Hb/cMWCNT-Fe_3O_4NP/CHIT/Au bioelectrode (curve iii) showed Hb binding as indicated by appearance of additional peak at 1,695 cm^{-1} assigned to the carbonyl stretch.

Electrochemical impedance measurements

Figure 7B shows electrochemical impedance spectra (EIS) of (a) bare Au electrode, (b) cMWCNT-Fe_3O_4NP/CHIT/Au electrode, and (c) Hb/cMWCNT-Fe_3O_4NP/CHIT/Au electrode. The charge transfer process in Hb/cMWCNT-Fe_3O_4NP/CHIT/Au electrode was studied by monitoring charge transfer resistance (R_{CT}) at the electrode and electrolyte interface. The value of the electron transfer resistance (semicircle diameter) (R_{CT}) depends on the dielectric and insulating features at the electrode/electrolyte interface. The R_{CT} values for bare Au electrode, cMWCNT-Fe_3O_4NP/CHIT/Au electrode and Hb/cMWCNT-Fe_3O_4NP/CHIT/Au electrodes were 650, 580, and 400 Ω, respectively. The composite electrode (cMWCNT-Fe_3O_4NP/CHIT/Au) showed better performance due to lower R_{CT} value (580 Ω) (Fig. 7B(b)) compared to bare electrode (R_{CT} value, 650 Ω) (Fig. 7B(a)). The working electrode (Hb/cMWCNT-Fe_3O_4NP/CHIT/Au) showed even better performance than composite electrode (cMWCNT-Fe_3O_4NP/CHIT/Au) due to the smooth electron transfer by Hb through its redox couple (Fe^{3+}/Fe^{2+}) and lowest R_{CT} value 400 Ω (Fig. 7B(c)). This decreased R_{CT} value in presence of Hb revealed that the electron transfer through redox couple was enhanced by the presence of Hb on the electrode surface.

Responses measurements of acrylamide biosensor

Acrylamide forms adduct with Hb, as a result of its interaction with $–NH_2$ group of the N-terminal valine of Hb [12].

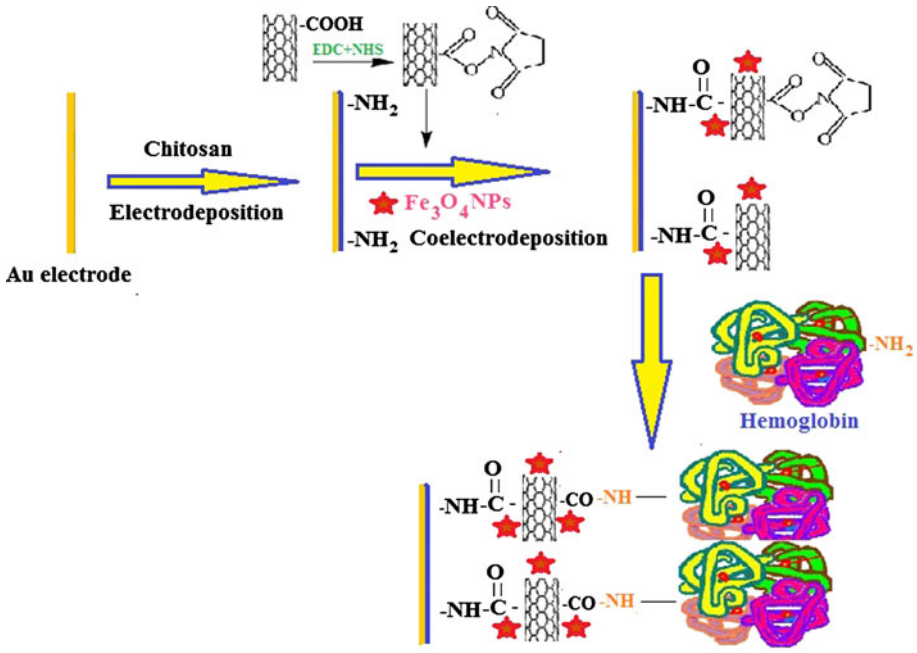

Fig. 4 Schematic representation of chemical reaction involved in the fabrication of Hb/cMWCNT-Fe_3O_4NP/CHIT/Au electrode

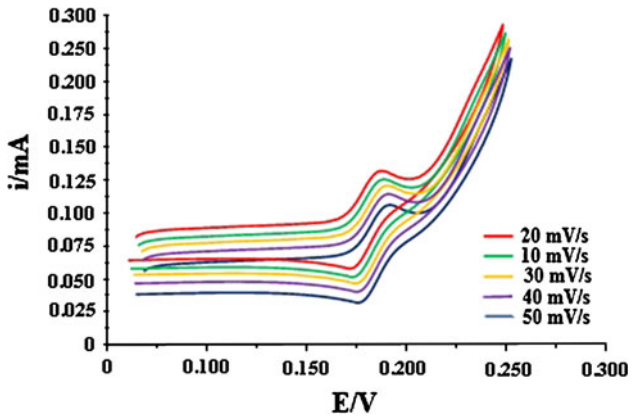

Fig. 5 Cyclic voltamogram for Hb/cMWCNT-Fe_3O_4NP/CHIT/Au electrode at different scan rates (i) 10 mV/s, (ii) 20 mV/s, (iii) 30 mV/s, (iv) 40 mV/s, (v) 50 mV/s: supporting electrolyte: 1 N KCl solution

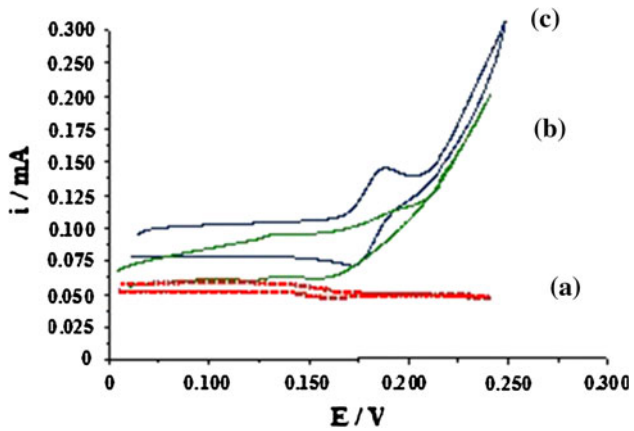

Fig. 6 Cyclic voltamogram for **a** bare Au, **b** CHIT/Au electrode, **c** cMWCNT-Fe_3O_4NP/CHIT/Au electrode. Supporting electrolyte: 1 N KCl solution; scan rate: 20 mV/s

Formation of this adduct is associated with Hb structure change [4]. This structure change is probably responsible for the decrease of accessibility of redox-active centers of Hb immobilized on the surface of the electrode, which causes a decrease of current. Hemoglobin-acrylamide adducts altered the electroactivity of Hb and generated lower response of the biosensor. Investigated cMWCNT-Fe_3O_4NP/CHIT/Au electrode modified with Hb displayed a quasi-reversible electrochemical reaction of Hb-Fe^{3+}/Hb-Fe^{2+}. The maximum response (current in mA) was observed at 0.182 V (Fig. 8a) and hence subsequent studies were carried out at this voltage. The optimum working potential of present acrylamide biosensor was lower than earlier reported amperometric acrylamide biosensor based on cMWCNT/CuNPs/PANI hybrid film (0.194 V) [14]. This biosensor displayed electrochemical response towards the acrylamide with a linear range 3–90 nM. As a consequence, in parallel with an increase of adduct hemoglobin–acrylamide concentration at the electrode surface, the current peak of DPV decreases (Fig. 8b). The results obtained show that a decrease of current can be treated as the analytical signal, and could be a base for very selective and sensitive acrylamide biosensors.

Optimization of biosensor

The optimum current was obtained at pH 5.0, which is almost similar to that of biosensor based on Hb-DDAB-modified

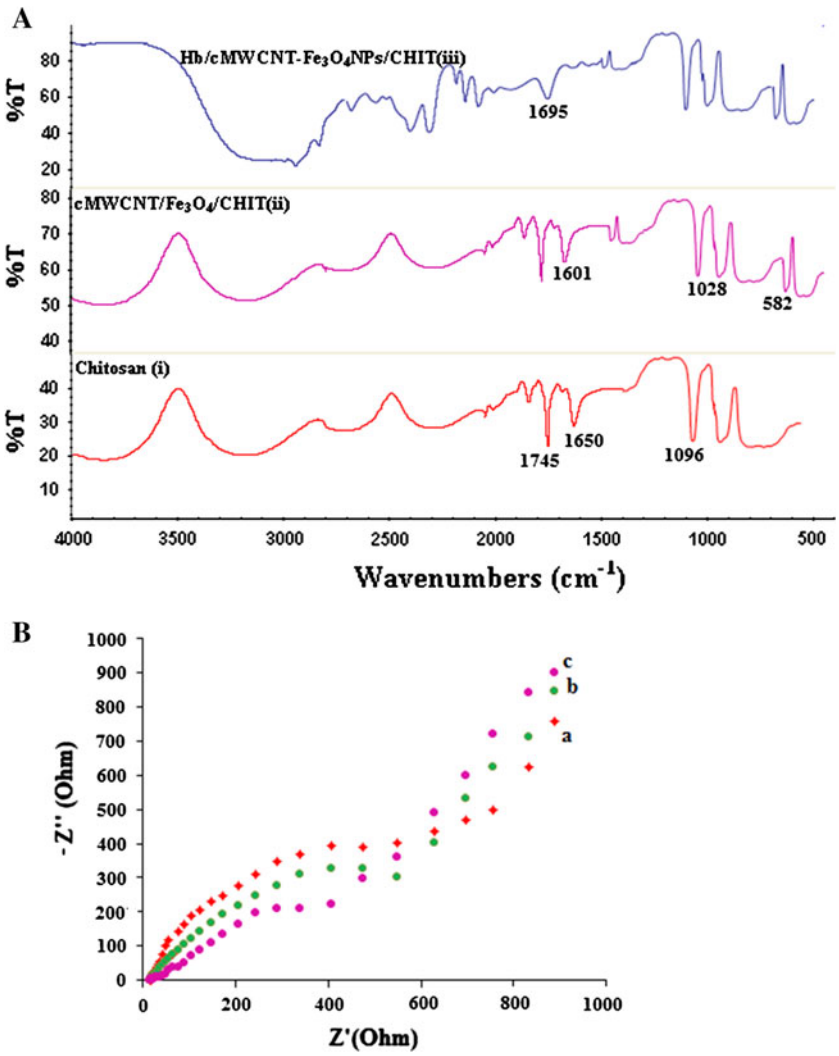

Fig. 7 **A** Fourier transform infera red spectra of CHIT/Au (i) cMWCNT-Fe_3O_4NP/CHIT/Au (ii) Hb/cMWCNT-Fe_3O_4NP/CHIT/Au electrode (iii), **B** Impedance spectra of (a) bare Au electrode (b) Hb/cMWCNT-Fe_3O_4NP/CHIT/Au electrode (c) cMWCNT-Fe_3O_4NP/CHIT/Au electrode in 5 mM $K_3Fe(CN)_6$:$K_4Fe(CN)_6$ (1:1)

carbon paste electrode (pH 4.8) [12] and biosensor based on GC electrodes modified with SWCNT/Hb (5.0) [13] and lower than biosensor based on cMWCNT/CuNPs/PANI hybrid film (5.5) [14]. The optimum temperature of biosensor was 30 °C, which is lower than biosensor based on cMWCNT/CuNPs/PANI hybrid film (5.5) [14]. There was a inverse hyperbolic relationship between biosensor response and acrylamide concentration in the range 3–130 nM. The response was constant after 90 nM (Fig. 1 inset).

Evaluation of biosensor

Linearity

There was a inverse linear relationship between the current (in μA) and the acrylamide concentration in the range 3–90 nM, which is a better linear range than those of earlier biosensor based on Hb-DDAB-modified carbon paste electrode (1.3×10^{-11}–4.8×10^{-5} M) [12], biosensor based on GC electrodes modified with SWCNT/Hb (1.0×10^{-11}–1.0×10^{-3} M) [13] and biosensor based on cMWCNT/CuNPs/PANI composite electrodeposited onto pencil graphite (PG) electrode (5 nM–75 mM) [14].

Detection limit

The detection limit of the present sensor was 0.02 nM (S/N = 3) with a sensitivity of 36.9 μA/nM/cm^2, which is lower than that for earlier biosensor based on Hb-DDAB-modified carbon paste electrode (1.2×10^{-10} M) [12], biosensor based on GC electrodes modified with SWCNT/Hb (1.0×10^{-9} M) [13] and biosensor based on cMWCNT/CuNPs/PANI composite electrodeposited onto pencil graphite (PG) electrode (0.2 nM) [14]. It might be due to the synergistic effect of CHIT, cMWCNT, and Fe_3O_4NPs in the fabrication of present working electrode, which facilitates the faster electron communication. Further the metallic nature of present electrode (Au) compared to previously used non-metallic electrode, has an advantage in flow of current.

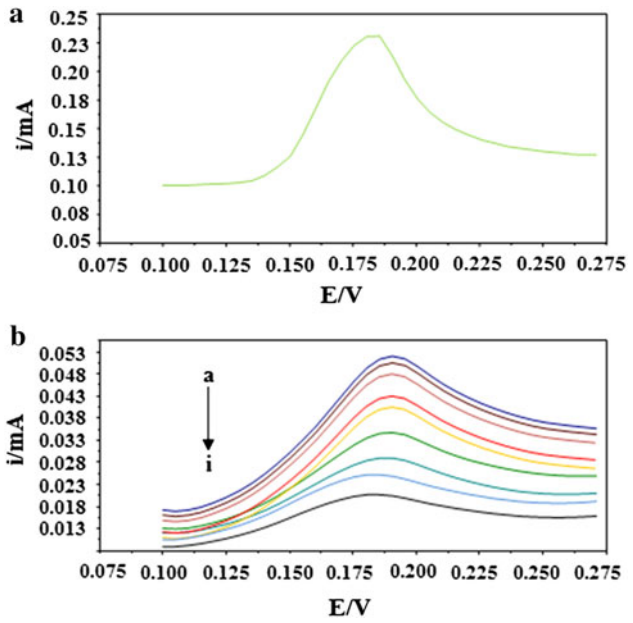

Fig. 8 **a** Differential pulse voltammogram for Hb/cMWCNT-Fe_3O_4NP/CHIT/Au electrode 3.5 μM acrylamide in 0.2 M sodium acetate buffer (pH 5.0) with scan rate 20 mVs^{-1}. **b** Differential pulse voltammogram measured with Hb/cMWCNT-Fe_3O_4NP/CHIT/Au containing different concentrations of acrylamide in a solution with 0.2 M sodium acetate buffer (pH 5.0); scan rate 20 mVs^{-1}

Table 1 Acrylamide levels in different brands of potato crisps as measured by Hb/cMWCNT-Fe_3O_4NP/CHIT/Au electrode

S.no.	Brand name	Acrylamide concentration (nM) (mean ± SD) ($n = 4$)
1	A	80.6 ± 0.3
2	B	72.9 ± 0.4
3	C	65.2 ± 0.2
4	D	48.3 ± 0.1

Analytical recovery

The average recoveries of acrylamide added to potato crisp water extract (at levels of 20 and 40 nM) varied from 95.40 to 97.56 %, demonstrating the high reliability of the present biosensor.

Precision

Within-sample and between-sample coefficients of variation (CVs) for the determination of acrylamide in potato crisps on the same day and after 1 week of storage were 2.2 and 4.3 %, respectively, indicating the good reproducibility and consistency of the present method. These results were better than those of biosensor based on cMWCNT/CuNPs/PANI composite electrodeposited onto pencil graphite (PG) electrode (2.35 and 4.50 %) [14], which can be attributed to the excellent immobilization of Hb onto the cMWCNT-Fe_3O_4NPs/CHIT/Au electrode.

Detection of acrylamide in potato crisps

Acrylamide levels as measured by the present biosensor ranged from 48.3 to 80.6 nM in potato crisps (Table 1). These values are comparable to those stated in earlier reports [12, 13].

Conclusion

An improved amperometric acrylamide biosensor was constructed by immobilization of Hb onto nanocomposite of cMWCNT and Fe_3O_4NPs electrodeposited onto Au electrode through CHIT film, which showed remarkably enhanced sensitivity and selectivity for acrylamide. The biosensor showed relatively rapid response, broad linear range, low detection limit (0.02 nM), good reproducibility, and long stability. This nanocomposite could also be used for improvement of analytical performance of other biosensors.

Acknowledgments Authors (Bhawna Batra) and (Suman Lata) are thankful to the Council of Scientific and Industrial Research (CSIR), India, for the award of Junior and Senior Research Fellowship during this study.

References

1. Ruden C (2004) Acrylamide and cancer risk—export risk assessments and the public debate. Food Chem Toxicol 42:335–349
2. Wilson KM, Mucci LA, Cho E, Hunter DJ, Chen WY, Willett WC (2009) Dietary acrylamide intake and risk of premenopausal breast cancer. Am J Epidemiol 169:954–961
3. Robert F, Vuataz G, Pollien P, Saucy F, Alonso MI, Bauwens I, Blank I (2005) Acrylamide formation from asparagine under low moisture Maillard reaction conditions. 2. Crystalline vs amorphous model systems. J Agric Food Chem 53:4628–4632
4. Erickson BE (2004) Finding acrylamide. Anal Chem 76:247A–248A
5. Mestdagh FJ, de Meulenaer B, Van Poucke C, Detavernier C, Cromphout C, Van Peteghem C (2005) Influence of oil type on the amounts of acrylamide generated in a model system and in French fries. J Agric Food Chem 53:6170–6174
6. Knol JJ, Van Loon WAM, Linssen JPH, Ruck AL, Van Boekel M, Voragen AGJ (2005) Toward a kinetic model for acrylamide formation in a glucose-asparagine reaction system. J Agric Food Chem 53:6133–6139
7. Wilde TD, Meulenaer BD, Mestdagh F, Govaert Y, Vandeburie S, Ooghe W, Fraselle S, Demeulemeester K, Peteghem CV, Calus A, Degroodt JM, Verh′e R (2005) Influence of storage practices on acrylamide formation during potato frying. J Agric Food Chem 53:6550–6557
8. Ros′en J, Helleñas KE (2002) Analysis of acrylamide in cooked foods by liquid chromatography tandem mass spectrometry. Analyst 127:880–882

9. Castele L (2003) Analytical methods for acrylamide determination in food. Qud-Turnhout, Belgium
10. Ono H, Chuda Y, Ohnishi-Kameyama M, Yada H, Ishizaka M, Kobayashi H, Yoshida M (2003) Analysis of acrylamide by LC-MS/MS and GC-MS in processed Japanese foods. Food Addit Contam 20:215–220
11. Zhang Y, Ren Y, Jiao J, Li D, Zhang Y (2011) Ultra high-performance liquid chromatography-tandem mass spectrometry for the simultaneous analysis of asparagine, sugars, and acrylamide in Maillard reactions. Anal Chem 83:3297–3304
12. Stobiecka A, Radecka H, Radecki J (2007) Novel voltammetric biosensor for determining acrylamide in food samples. Biosens Bioelectron 22:2165–2170
13. Krajewska A, Radecki J, Radecka H (2008) A voltammetric biosensor based on glassy carbon electrodes modified with single-walled carbon nanotubes/hemoglobin for detection of acrylamide in water extracts from potato crisps. Sensors 8:5832–5844
14. Batra B, Lata S, Sharma M, Pundir CS (2013) An acrylamide biosensor based on immobilization of hemoglobin onto multi-walled carbon nanotube/copper nanoparticles/polyaniline hybrid film. Anal Biochem 433:210–217
15. Zhang H, Neau SH (2001) In vitro degradation of chitosan by a commercial enzyme preparation: effect of molecular weight and degree of deacetylation. Biomaterials 22:1653–1658
16. Wang Y, Zhang X, Chen Y, Xu H, Tan Y, Wang S (2010) Detection of dopamine based on tyrosinase-Fe_3O_4 nanoparticles-chitosan nanocomposite biosensor. Am J Biomed Sci 2:209–216
17. Mohapatra M, Anand S (2010) Synthesis and applications of nano-structured iron oxides/hydroxides—a review. Inter J Eng Sci Technol 2:127–146
18. Kim DK, Mikhaylova M, Zhang Y, Muhammed M (2003) Protective coating of superparamagnetic iron oxide nanoparticles. Chem Mater 15:1617–1627